Journal of the Physical Society of Japan
Vol. 78, No. 4, April, 2009, 043706

Checkerboard States in the Two-Dimensional Hubbard Model with the Bi2212-Type Band

Mitake MIYAZAKI, Kunihiko YAMAJI[1], Takashi YANAGISAWA[1], and Ryosuke KADONO[2]

Hakodate National College of Technology, 14-1 Tokura-cho, Hakodate, Hokkaido 042-8501
[1]*Nanoelectronics Research Institute, AIST, Central 2, 1-1-1 Umezono, Tsukuba, Ibaraki 305-8568*
[2]*Institue of Materials Structure Science, KEK, Tsukuba, Ibaraki 305-0801*

(Received December 26, 2008; accepted February 9, 2009; published March 25, 2009)

We have performed a variational Monte Carlo simulation on a two-dimensional t–t'–t''–U Hubbard model with a Bi-2212-type band to examine the stability of a 4×4 checkerboard state, which has been observed recently by scanning tunneling microscopy (STM) in Bi-2212 and Na-CCOC. The condensation energies of inhomogeneous magnetic and charge-ordered states at 1/8 hole doping are calculated. We found that the coexistent state of bond-centered four-period diagonal and vertical spin-checkerboard structures characterized by a multi-$\boldsymbol{Q}$ set is stabilized and composed of 4×4 period checkerboarded spin modulation. This state can be understood as an incommensurate spin density wave enhanced by Fermi surface nesting, which appears in the precursory peaks of spin susceptibility at $\sim(\pi,\pi/2)$, $(\pi/2,\pi)$, and $(\pi/2,\pi/2)$.

KEYWORDS: two-dimensional Hubbard model, checkerboard state, stripe state, cuprate, Bi-2212, variational Monte Carlo method
DOI: 10.1143/JPSJ.78.043706

The realization of incommensurate electron states in the under-doped region of high-T_c cuprates has attracted considerable interest recently. Several experimental reports indicated that the stripe state is stabilized in La-based cuprates: From elastic neutron scattering experiments on $La_{2-x-y}Nd_ySr_xCuO_4$,[1] $La_{2-x}Sr_xCuO_4$ (LSCO),[2] and $La_{2-x}Ba_xCuO_4$,[3] incommensurate magnetic peaks have been observed at $(\pi,\pi\pm\epsilon)$ or $(\pi\pm\epsilon,\pi)$. A checkerboard-like charge-density modulation with a roughly $4a\times4a$ period (a is a lattice spacing) has also been observed by scanning tunneling microscopy (STM) experiments in $Bi_2Sr_2CaCu_2O_{8+\delta}$ (Bi-2212),[4] $Bi_2Sr_{2-x}La_xCuO_{6+\delta}$,[5] and $Ca_{2-x}Na_xCuO_2Cl_2$ (Na-CCOC).[6] It is important whether or not these inhomogeneous electrons can be understood within the framework of strongly or moderately correlated electrons.

A two-dimensional Hubbard model is appropriate for cuprates. As it is pointed out by variational Monte Carlo (VMC) calculation,[7] this model gives the condensation energy of the superconducting state of the correct order of the experimental one.[8,9] The theoretical study of possible inhomogeneous states in this model was started almost 20 years ago. It was discussed by using the mean field theory[10–14] that a striped incommensurate spin density wave (ISDW) state and a charge density wave (ICDW) state appear when an incommensurate nesting becomes favorable in a hole-doped Hubbard band. It was shown by VMC calculation[15] that the striped ISDW wave function gives much better variational energies than the commensurate SDW wave function. The later VMC studies[16,17] indicated that the coexistent state of the superconductivity and the striped ISDW is more stabilized in an under-doping region, simultaneously explaining the relationship between the hole density and the incommensurability in neutron scattering data for La-based cuprates. The latter relationship was reported to be found also in the t–J[18] and d–p[19] models.

Possible several electronic checkerboard states have been proposed theoretically.[20–22] The density matrix renormalization group calculation performed on small t–J clusters found that a 4×4 checkerboard-like charge modulation appears on an eight-period vertical stripe background.[20] A Hartree–Fock calculation assuming the appropriate band parameters of Bi-2212 and Na-CCOC revealed that Fermi surface nesting leads to an eight-period double-$\boldsymbol{Q}$ diagonal ISDW instability, which is accompanied by a 4×4 checkerboarded ICDW order.[21] Similar spin and charge distributions were obtained by Seibold *et al.* as the stable solution of a t–t'–U Hubbard model in an unrestricted Gutzwiller approximation study.[22] They argued that the checkerboard pattern emerges owing to a kinetic energy gain on the 2×2 ferromagnetic plaquettes formed by the intersection of striped domain walls. However, whether different orders compete or cooperate still remains controversial.

The present study was undertaken to determine possible inhomogeneous electron states in a two-dimensional (2D) t–t'–t''–U Hubbard model,

$$\hat{H} = -\sum_{i,j,\sigma} t_{ij}(\hat{c}^{\dagger}_{i\sigma}\hat{c}_{j\sigma} + \text{h.c.}) + U\sum_i \hat{n}_{i\uparrow}\hat{n}_{i\downarrow}, \tag{1}$$

where the transfer energy $t_{ij} = t$, t', t'', and 0, if sites i and j are first-, second-, third-nearest neighbor and otherwise, respectively. In the following, we consider t as the unit of energy. $\hat{c}^{\dagger}_{i\sigma}$ ($\hat{c}_{i\sigma}$) is the creation (annihilation) operator of the electron with spin σ (↑ or ↓) at site i ($i = 1,\ldots,N_{\text{site}}$) and $\hat{n}_{i\sigma} = \hat{c}^{\dagger}_{i\sigma}\hat{c}_{i\sigma}$. U is the on-site Coulomb energy.

In the VMC calculation, the variational energy is written as,

$$E_{\text{var}} = \frac{\langle\Psi|\hat{H}|\Psi\rangle}{\langle\Psi|\Psi\rangle}. \tag{2}$$

We use the trial wave function $|\Psi\rangle$ defined by

$$|\Psi\rangle = \hat{P}_{N_e}\hat{P}_G\hat{P}_J|\phi_{\text{HF}}\rangle, \tag{3}$$

where $\hat{P}_{N_e}$ is a projection operator that extracts only the components with a fixed total electron number N_e. $\hat{P}_G$ is the Gutzwiller projection operator given by $\hat{P}_G = \prod_i[1-(1-g)\hat{n}_{i\uparrow}\hat{n}_{i\downarrow}]$, where g is a variational parameter in the

range from 0 to unity, which controls the on-site electron correlation. $\hat{P}_{\rm J}$ is the Jastrow-type projection operator $\hat{P}_{\rm J} = \prod_{\langle ij \rangle} h^{\hat{n}_i \hat{n}_j}$, which allows the occupancy of the nearest-neighbor sites to be modified by adjusting h in the neighborhood of 1. $|\phi_{\rm HF}\rangle$ is a Hartree–Fock wave function for an inhomogeneous state. The Hartree–Fock Hamiltonian for ISDW with ICDW, which gives the Hartree–Fock solution $|\phi_{\rm HF}\rangle$, is represented by

$$\hat{H}_{\rm HF} = \sum_{ij\sigma}(-t_{ij} - \mu)\hat{c}^{\dagger}_{i\sigma}\hat{c}_{j\sigma} + \frac{U}{2}\sum_{i\sigma}[\rho_i + {\rm sgn}(\sigma)m_i]\hat{n}_{i\sigma}, \quad (4)$$

where t_{ij} is defined as that in eq. (1) and μ is the chemical potential. The charge density ρ_i and spin density m_i are spatially modulated as

$$\rho_i = \sum_l \rho_l \cos[\boldsymbol{Q}^{\rm c}_l \cdot (\boldsymbol{r}_i - \boldsymbol{r}_0)], \quad (5)$$

$$m_i = \sum_l m_l \cos[\boldsymbol{Q}^{\rm s}_l \cdot (\boldsymbol{r}_i - \boldsymbol{r}_0)], \quad (6)$$

where ρ_l and m_l are variational parameters.

The striped ISDW state is defined by a single-$\boldsymbol{Q}$ set; the wave vector $\boldsymbol{Q}^{\rm s} = (\pi, \pi \pm 2\pi\delta)$ [or $(\pi \pm 2\pi\delta, \pi)$] produces the spin vertical stripe (spin-VS) state in which magnetic domains run along the x-direction (y-direction). δ is an incommensurability defined by the inverse of the stripe period in the y-direction. $\boldsymbol{r}_0$ represents the position of a magnetic domain wall. The site-centered (bond-centered) domain boundary is located on site (between sites); $\boldsymbol{r}^{\rm SC}_0 = (0,0)$ $[\boldsymbol{r}^{\rm BC}_0 = (1/2, 1/2)]$. Note that the hole density is maximal on the domain wall. The charge-VS period is one-half the spin-VS period, i.e., $\boldsymbol{Q}^{\rm c} = 2\boldsymbol{Q}^{\rm s} = (2\pi, 2\pi \pm 4\pi\delta)$. The diagonal stripe (DS) state with the diagonal wave vector $\boldsymbol{Q}^{\rm s}$ $[= (\pi \pm 2\pi\delta, \pi \pm 2\pi\delta)]$ and $\boldsymbol{Q}^{\rm c}$ $(= 2\boldsymbol{Q}^{\rm s})$ can be treated in the same manner.

On the other hand, the checkerboarded ISDW state is described by the double-$\boldsymbol{Q}$ set.[21,23] For example, vertical wave vectors $\boldsymbol{Q}^{\rm s}_1 = (\pi, \pi \pm 2\pi\delta)$ and $\boldsymbol{Q}^{\rm s}_2 = (\pi \pm 2\pi\delta, \pi)$ describes a spin vertical checkerboard (spin-VC) state, where two diagonal domain walls are orthogonal, as discussed in ref. 23. While, diagonal wave vectors $\boldsymbol{Q}^{\rm s}_1 = (\pi \pm 2\pi\delta, \pi \pm 2\pi\delta)$ and $\boldsymbol{Q}^{\rm s}_2 = (\pi \pm 2\pi\delta, \pi \mp 2\pi\delta)$ lead to a spin diagonal checkerboard (spin-DC) state with a $1/\delta$-period. The magnetic domain walls run parallel to both x- and y-directions. Then, the hole density forms the charge vertical checkerboard (charge-VC) pattern with vertical wave vectors $\boldsymbol{Q}^{\rm c}_1 = (0, \pm 4\pi\delta)$ and $\boldsymbol{Q}^{\rm c}_2 = (2\pi \pm 4\pi\delta, 2\pi)$ in which the hole density is maximal on the crossing point of magnetic domain walls in the spin-DC state. If $\delta = 1/8$ is assumed as suggested in previous studies,[21,22] the charge modulation pattern is consistent with the 4a×4a charge structure observed in STM experiments. In the following, we examine the energy gain of the eight-period spin-DC state with the four-period charge-VC pattern and compare it with other states.

The energy expectation values, eq. (2), are optimized with a total Monte Carlo step number greater than 3×10^7. In this study, we fix the on-site Coulomb energy $U = 8$ and adopt the square lattices $L \times L$ ($L = 8-20$); the commensurability with δ is required to guarantee the spin-periodicity along both x- and y-direction in the $1/\delta$-period spin-checkerboarded ISDW state. The periodic boundary conditions in both directions are applied.

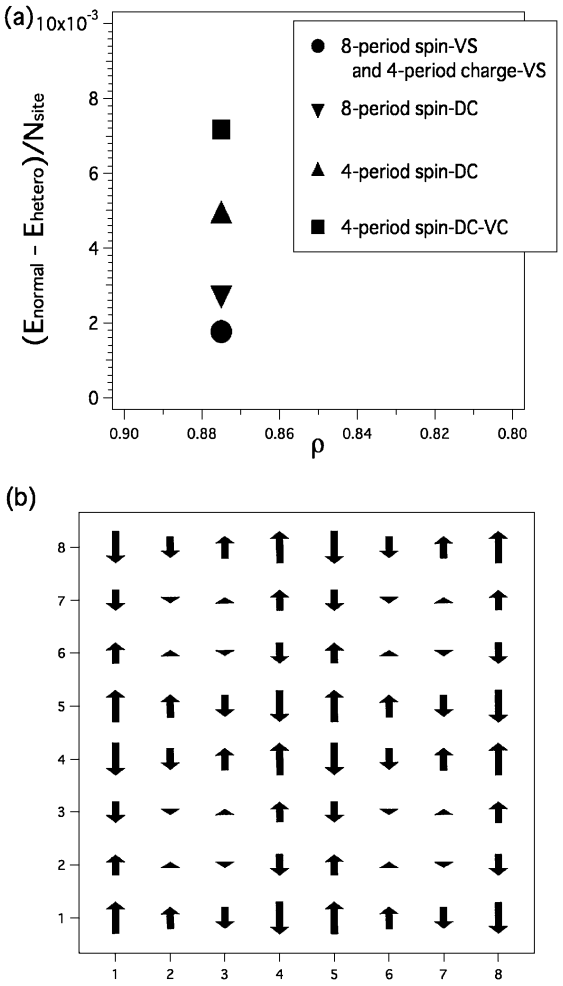

Fig. 1. (a) Condensation energies of inhomogeneous states with the bond-centered magnetic domain wall. The system is a 16×16 lattice in the Hubbard model with $t' = -0.32$, $t'' = 0.22$, and $U = 8$ for the case of $\rho = 0.875$. The static error bars are smaller than the size of symbols. (b) Expectation value of $\langle m_i \rangle$ measured in the four-period spin-DC–VC solution. The length of arrows is proportional to the spin density.

In Fig. 1(a), we show the condensation energies of some heterogeneous states, $(E_{\rm normal} - E_{\rm hetero})/N_{\rm site}$, fixing the transfer energies $t' = -0.32$ and $t'' = 0.22$ suitable for Bi-2212. The energy of the normal state $E_{\rm normal}$ is calculated by assuming $m_l = \rho_l = 0$ in eq. (4). The system used is a 16×16 lattice with the electron-filling $\rho = N_{\rm e}/N_{\rm site} = 0.875$. In our calculation, the condensation energies of both bond-centered stripe and checkerboard states are always larger than those of site-centered stripe and checkerboard states. The VS state is not stable in this parameter set, which is only stabilized with the LSCO-type band, as shown later. The four-period spin-DC state is significantly more stable than the eight-period spin-DC state, or 6-, 10-, 12-, and 16-period spin-DC states [these are not shown in Fig. 1(a)]. Moreover, the trial wave function is improved on the basis of the consideration stated later. We found that the coexistent state of the bond-centered four-period spin-DC and four-period spin-VC with the assumed $\rho_l = 0$ is the most stable, as shown in Fig. 1(a). Note that the condensation energy of the coexistent state is several times larger than the super-

conducting energy calculated in the optimal doping on the same system size.[24)]

This state is described by two sets of $\boldsymbol{Q}$; the spin density is spatially modulated as

$$m_i = m_{\mathrm{D}}\{\cos[\boldsymbol{Q}_1^{\mathrm{s}} \cdot (\boldsymbol{r}_i - \boldsymbol{r}_0^{\mathrm{BC}})] + \cos[\boldsymbol{Q}_2^{\mathrm{s}} \cdot (\boldsymbol{r}_i - \boldsymbol{r}_0^{\mathrm{BC}})]\} + m_{\mathrm{V}}\{\cos[\boldsymbol{Q}_3^{\mathrm{s}} \cdot (\boldsymbol{r}_i - \boldsymbol{r}_0^{\mathrm{BC}})] + \cos[\boldsymbol{Q}_4^{\mathrm{s}} \cdot (\boldsymbol{r}_i - \boldsymbol{r}_0^{\mathrm{BC}})]\}, \quad (7)$$

where m_{D} and m_{V} are the magnetizations of the spin-DC and spin-VC states, respectively. The first and second terms on the right-hand side of eq. (7) are characterized by the $\{\boldsymbol{Q}_1^{\mathrm{s}} = (\pi \pm \pi/2, \pi \pm \pi/2),\ \boldsymbol{Q}_2^{\mathrm{s}} = (\pi \pm \pi/2, \pi \mp \pi/2)\}$ and $\{\boldsymbol{Q}_3^{\mathrm{s}} = (\pi \pm \pi/2, \pi),\ \boldsymbol{Q}_4^{\mathrm{s}} = (\pi, \pi \pm \pi/2)\}$ sets, respectively. The measured expectation value of the spin density $\langle m_i \rangle$ is shown in Fig. 1(b). The four-period spin structure appears along both x- and y-directions. It can be seen as the checkerboard pattern consisting of 2×2 antiferromagnetic (AF) plaquettes, where magnetic moments of each spin in plaquettes are ∼0.5, 0.3, and 0.1. These values are smaller than the maximum local spin moment (∼0.8) of the vertical stripe state with $t' = -0.12$ and $t'' = 0.08$ suitable for LSCO.

Furthermore, charge amplitudes ρ_l are considered in order to exhibit the appropriate charge distribution in the four-period spin-DC–VC background. However, optimized ρ_l become almost zero among some inhomogeneous charge textures. When the expectation value of the charge density $\langle n_i \rangle$ is measured under the condition of $\rho_l = 0$, charge stripes passing through the 2×2 AF plaquette with small magnetic moments appear. However, the slight difference observed among variational parameters leads to a type of inhomogeneous charge texture (e.g., horizontal or longitudinal charge stripe or charge checkerboard). In addition, the charge amplitude is very small: the deviation from the mean charge value is ∼2%, compared with the VS case of $t' = -0.12$ and $t'' = 0.08$, where the charge density varies in the range of 0.80–0.93. Therefore, it seems that the charge order state is energetically unstable because excess charges cannot gain the kinetic energy so as to overcome Coulomb repulsion at around small AF plaquettes.

To investigate the instability towards the four-period spin-DC–VC state, the susceptibility $\chi_0(\boldsymbol{Q})$ with $U = 0$ is calculated in the case of $t' = -0.32$, $t'' = 0.22$, and $\rho = 0.875$. As shown in Fig. 2(b), the peak at $(0.45\pi, 0.45\pi)$ and ridges linking $(\pi, \pi/2)$ and $(\pi/2, \pi)$ are observed. These features can be understood by the nesting between parts of the Fermi surface; the peak at $(0.45\pi, 0.45\pi)$ corresponds to $\boldsymbol{Q}_1$ and $\boldsymbol{Q}_2$, and peaks at $(\pi/2, \pi)$ and $(\pi, \pi/2)$ correspond to $\boldsymbol{Q}_3$ and $\boldsymbol{Q}_4$, respectively. [Fig. 2(d)]. This indicates that the four-period spin-DC and four-period spin-VC states are enhanced by nesting with the $\{\boldsymbol{Q}_1, \boldsymbol{Q}_2\}$ and $\{\boldsymbol{Q}_3, \boldsymbol{Q}_4\}$ sets, respectively. On the other hand, as a reference, we show the susceptibility in the case of $t' = -0.12$ and $t'' = 0.08$ in Fig. 2(a). It was already discussed in the mean field study[14)] that the VS structure is driven by Fermi surface nesting, such as that shown in Fig. 2(c). The wave vector $\boldsymbol{Q}_{\mathrm{VS}} = (\pi, \pi \pm \pi/4)$ or $(\pi \pm \pi/4, \pi)$ of the eight-period spin-VS state is considered to come from peaks in the ridges in $\chi_0(\boldsymbol{Q})$, as shown in Fig. 2(a). Although the highest point is at (π, π) in $\chi_0(\boldsymbol{Q})$, the eight-period striped ISDW state is markedly more stable than the commensurate SDW state in our VMC calculation.

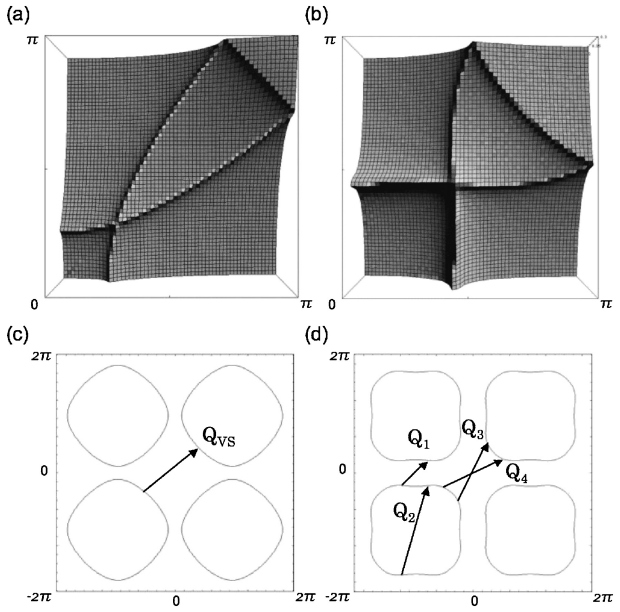

Fig. 2. Non interacting susceptibility $\chi_0(\boldsymbol{Q})$ with $\rho = 0.875$ for the cases of (a) $t' = -0.12$ and $t'' = 0.08$, and (b) $t' = -0.32$ and $t'' = 0.22$. Non interacting Fermi surface with $\rho = 0.875$ for the cases of (c) $t' = -0.12$ and $t'' = 0.08$, and (d) $t' = -0.32$, $t'' = 0.22$. The nesting wave vectors $\boldsymbol{Q}_{\mathrm{VS}} \sim (\pi, 0.875\pi)$ and $\{\boldsymbol{Q}_1 \sim (\pi/2, \pi/2),\ \boldsymbol{Q}_2 \sim (\pi/2, 3\pi/2),\ \boldsymbol{Q}_3 = (\pi/2, \pi),\ \boldsymbol{Q}_4 = (\pi, \pi/2)\}$ are illustrated in (c) and (d), respectively.

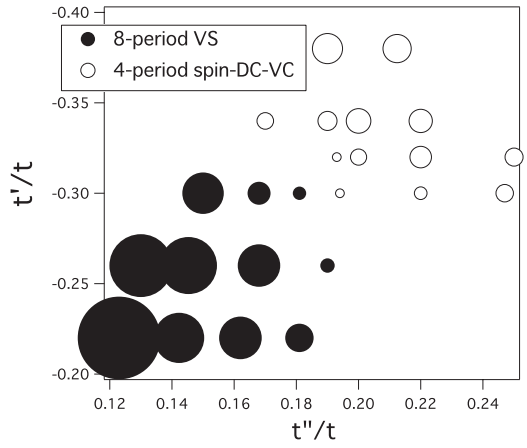

Fig. 3. Phase diagram on the plane of t' and t'' obtained from the condensation energies on the 16×16 lattices for the case of $U = 8$ and $\rho = 0.875$. The radius of circles is proportional to the values of the condensation energy.

Figure 3 shows the t' and t'' dependences of the condensation energies of the most stable inhomogeneous state at $\rho = 0.875$. The radius of circles represents the magnitude of the calculated condensation energy. The four-period spin-DC–VC state appears in the large $|t'|$–t'' region suitable for Bi-2212, where the peak around $(\pi/2, \pi/2)$ is predominant in $\chi_0(\boldsymbol{Q})$, as mentioned above. For example, the radius for the case of $t' = -0.38$ and $t'' = 0.19$ corresponds to 0.010. The VS state with single-$\boldsymbol{Q}$ is fairly stable in the small $|t'|$–t'' region, and the condensation energy of the VS state for $t' = -0.12$ and $t'' = 0.08$ is ∼0.043. These results can be explained from the significant enhancement of $\chi_0(\boldsymbol{Q})$ at incommensurate positions around (π, π). As $|t'|$ and t'' increase, the incommensurate peak intensities of $\chi_0(\boldsymbol{Q})$ and the condensation energy of the VS state decrease. If we

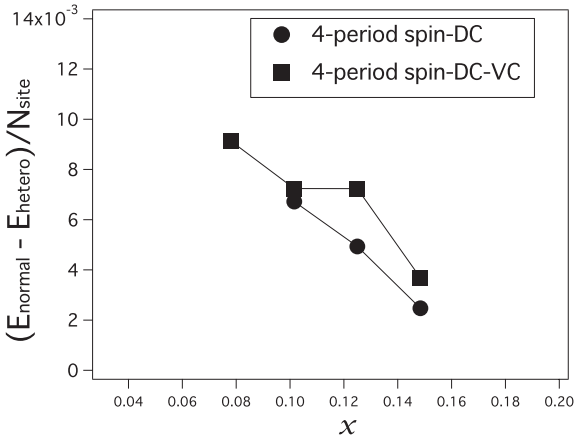

Fig. 4. Hole density dependence of the condensation energies of the four-period spin-DC–VC and spin-DC states. The system is a 16×16 lattice for the case of $t' = -0.32$, $t'' = 0.22$, and $U = 8$.

assume $t'' = -t'/2$ following ref. 25, the phase transition from the VS state to the four-period spin-DC–VC state occurs at $t' \sim -0.32$. The magnetic structure of the system is mainly characterized by the wave vector not around (π, π) but around $(\pi/2, \pi/2)$. In the $|t'| < 0.32$ region, the expectation values of both the charge and spin amplitudes of the four-period VS state are hardly affected by the shape of the Fermi surface. However, in the $|t'| > 0.32$ region, the charge amplitude becomes zero and only spin modulation remains accompanying the change from a 1D spin-striped structure to a 2D spin-checkerboarded structure.

In Fig. 4, the condensation energies are shown as a function of the hole density x. The four-period spin-DC–VC state grows as hole doping level decreases, which can be understood in terms of the nesting condition with $\boldsymbol{Q}_1$: The peak around $(\pi/2, \pi/2)$ in $\chi_0(\boldsymbol{Q})$ is enhanced by a decrease in hole doping level. It seems that the shoulder structure around $x = 0.125$ in Fig. 4 originates from the nesting effect with $\boldsymbol{Q}_3$ and $\boldsymbol{Q}_4$, since the position of the ridges in $\chi_0(\boldsymbol{Q})$ shifts from $(\pi, \pi/2)$ and $(\pi/2, \pi)$ when hole density changes from 0.125. Therefore, the four-period spin-DC–VC state changes to the four-period spin-DC state with equivalent AF plaquettes when doping level becomes lower the underdoped region. We also found that the system with large $|t'|$ and t'' values maintains the four-period spin-DC–VC state (or four-period spin-DC state) stably in contrast to the small $|t'|$–t'' phase, where the period of the stripe state with the maximum condensation energy gradually decreases as the hole density increases.[16)]

In summary, the ground state of the 2D Hubbard model with a Bi-2212-type band was investigated by using the VMC method. The condensation energies of some inhomogeneous magnetic and charge-ordered states at 1/8 hole doping were calculated. We found that the four-period spin-DC–VC state without charge modulation is stabilized. This state composed of 2×2 AF plaquettes exhibits a checkerboard-like spin modulation with a 4×4 period, which comes from the multi-$\boldsymbol{Q}$ set [i.e., $\boldsymbol{Q}_1^{\mathrm{s}} = (\pi \pm \pi/2, \pi \pm \pi/2)$, $\boldsymbol{Q}_2^{\mathrm{s}} = (\pi \pm \pi/2, \pi \mp \pi/2)$, $\boldsymbol{Q}_3^{\mathrm{s}} = (\pi, \pi \pm \pi/2)$, and $\boldsymbol{Q}_4^{\mathrm{s}} = (\pi \pm \pi/2, \pi)$]. It can be considered that these wave vectors correspond to the peaks in susceptibility with $U = 0$. To our knowledge, this multiple-$\boldsymbol{Q}$ SDW state gives the lowest energy among variational wave functions proposed so far. It is an interesting problem whether or not a 4×4 charge-checkerboard pattern is induced by local spin-lattice coupling associated with the spin distortion of 2×2 AF plaquettes.

Acknowledgment

This work is supported by the Large Scale Simulation Program No. 08-11 (FY2008) of High Energy Accelerator Research Organization (KEK).

1) J. M. Tranquada, J. D. Axe, N. Ichikawa, Y. Nakamura, S. Uchida, and B. Nachumi: Phys. Rev. B **54** (1996) 7489.
2) T. Suzuki, T. Goto, K. Chiba, T. Shinoda, T. Fukase, H. Kimura, K. Yamada, M. Ohashi, and Y. Yamaguchi: Phys. Rev. B **57** (1998) R3229.
3) M. Fujita, H. Goka, T. Adachi, Y. Koike, and K. Yamada: Physica C **426–431** (2005) 257.
4) J. E. Hoffman, E. W. Hudson, K. M. Lang, V. Madhavan, H. Eisaki, S. Uchida, and J. C. Davis: Science **295** (2002) 466.
5) W. D. Wise, M. C. Boyer, K. Chatterjee, T. Kondo, T. Takeuchi, H. Ikuta, Y. Wang, and E. W. Hudson: Nat. Phys. **4** (2008) 696.
6) T. Hanaguri, C. Lupien, Y. Kohsaka, D. H. Lee, M. Azuma, M. Takano, H. Takagi, and J. C. Davis: Nature (London) **430** (2004) 1001.
7) K. Yamaji, T. Yanagisawa, M. Miyazaki, and R. Kadono: Physica C **468** (2008) 1125.
8) Z. Hao, J. R. Clem, M. W. McElfresh, L. Civale, A. P. Malozemoff, and F. Holtzberg: Phys. Rev. B **43** (1991) 2844.
9) J. W. Loram, K. A. Mirza, J. R. Cooper, and W. Y. Liang: Phys. Rev. Lett. **71** (1993) 1740.
10) K. Machida: Physica C **158** (1989) 192.
11) D. Poilblanc and T. M. Rice: Phys. Rev. B **39** (1989) 9749.
12) H. J. Schulz: J. Phys. (Paris) **50** (1989) 2833.
13) J. Zaanen and O. Gunnarsson: Phys. Rev. B **40** (1989) 7391.
14) M. Ichioka and K. Machida: J. Phys. Soc. Jpn. **68** (1999) 4020.
15) T. Giamarchi and C. Lhuillier: Phys. Rev. B **42** (1990) 10641.
16) M. Miyazaki, K. Yamaji, and T. Yanagisawa: J. Phys. Chem. Solids **63** (2002) 1403.
17) M. Miyazaki, T. Yanagisawa, and K. Yamaji: J. Phys. Soc. Jpn. **73** (2004) 1643.
18) A. Himeda, T. Kato, and M. Ogata: Phys. Rev. Lett. **88** (2002) 117001.
19) T. Yanagisawa, S. Koike, M. Miyazaki, and K. Yamaji: J. Phys.: Condens. Matter **14** (2002) 21.
20) S. R. White and D. J. Scalapino: Phys. Rev. B **70** (2004) 220506.
21) M. Takigawa: J. Phys. Chem. Solids **67** (2006) 391.
22) G. Seibold, J. Lorenzana, and M. Grilli: Phys. Rev. B **75** (2007) 100505(R).
23) M. Kato, K. Machida, H. Nakanishi, and M. Fujita: J. Phys. Soc. Jpn. **59** (1990) 1047.
24) K. Yamaji, T. Yanagisawa, and S. Koike: Physica B **284–288** (2000) 415.
25) E. Pavarini, I. Dasgupta, T. Saha-Dasgupta, O. Jepsen, and O. K. Andersen: Phys. Rev. Lett. **87** (2001) 047003.